

# The PointGroupNRG code for numerical renormalization group calculations with discrete point-group symmetries.

Aitor Calvo-Fernández<sup>a,b</sup>, María Blanco-Rey<sup>c,b,d</sup>, Asier Eiguren<sup>a,b,e</sup>

<sup>a</sup> *Departamento de Física, Universidad del País Vasco UPV-EHU, 48080 Leioa, Spain*

<sup>b</sup> *Donostia International Physics Center (DIPC), 20018 Donostia-San Sebastián, Spain*

<sup>c</sup> *Departamento de Polímeros y Materiales Avanzados: Física, Química y Tecnología, Universidad del País Vasco UPV-EHU, 20018 Donostia-San Sebastián, Spain*

<sup>d</sup> *Centro de Física de Materiales CFM/MPC (CSIC-UPV/EHU), Paseo Manuel de Lardizábal 5, 20018 Donostia-San Sebastián, Spain*

<sup>e</sup> *EHU Quantum Center, University of the Basque Country UPV/EHU, 48940 Leioa, Spain*

---

## Abstract

The numerical renormalization group (NRG) has been widely used as a magnetic impurity solver since the pioneering works by Wilson. Over the past decades, a significant attention has been focused on the application of symmetries in order to reduce the computational cost of the calculations and to improve their accuracy. In particular, a notable progress has been made in implementing continuous symmetries such as  $SO(3)$ , useful for studying impurities in an isotropic medium, or  $SU(N)$ , which is applicable to a wide range of systems. In this work, we focus on the application of discrete point group symmetries, which are particularly relevant for impurity systems in metals where crystal field effects are important. With this aim, we have developed an original NRG code written in the Julia language, `PointGroupNRG`, where we have implemented crystal point-group symmetries for the Anderson impurity model, as well as the continuous spin and charge symmetries. Among other results, we demonstrate the advantage of our procedure by applying the code to a two-impurity model with RKKY interaction and an impurity system with two orbitals of  $E_g$  symmetry and two channels. We also provide benchmarks to show the performance improvements obtained by exploiting the orbital symmetries.

*Keywords:* numerical renormalization group, Anderson model, discrete

## 1. Introduction

The Numerical Renormalization Group (NRG) is a non-perturbative method pioneered by K. G. Wilson to solve the single-channel spin-1/2 Kondo model, which consists of a spin degree of freedom coupled to a bath of conduction electrons [1]. The method was devised in order to overcome the limitations of the perturbative treatment of the Kondo model, which results in infrared divergences for various physical quantities [2]. The strategy followed by the NRG is to perform a logarithmic discretization of the continuum of conduction degrees of freedom, dividing it into intervals  $[\Lambda^{-(n+1)}, \Lambda^{-n}]$  and  $[-\Lambda^{-n}, -\Lambda^{-(n+1)}]$  for  $n = 0, 1, 2, \dots$  for a discretization parameter  $\Lambda > 1$ , where the coupling terms introduced by each of these intervals decrease exponentially with  $n$ . The NRG method proceeds from the highest-energy excitations to the lowest energy scales by iteratively adding these intervals to the Hamiltonian, diagonalizing it, and discarding the highest-energy states.

Since its first implementation, the NRG method has seen improvements and extensions in various aspects. Some limitations of the original discretization scheme have been overcome by utilizing, for instance, a non-orthogonal conduction basis that removes the artificial renormalization of the impurity-band hybridization [3] or an adaptive discretization mesh that allows for a more accurate modeling of conduction bands with a non-constant density of states [4]. Other methodological developments have been aimed at alleviating the computational cost of the calculations, which becomes an obstacle as the number of impurities or the degrees of freedom of the impurity and the bath increase. One improvement in this respect is the combination of calculations performed for various interleaved discretizations, which allows to use large values of the discretization parameter  $\Lambda$  and, at the same time, obtain smooth spectral functions [5] and thermodynamic functions [6]

Another line of improvement, which we follow in this work, is the application of symmetries. Symmetries have been implemented in the NRG method since the earliest works. In the seminal paper by Krishna-Murthy et al. [7], charge and spin symmetries were used in order to reduce the computational cost of the calculations, which were performed for a single-orbital, single-channel Anderson model. The extension of the NRG to more complex models, often featuring more degrees of freedom, has motivated the implementation of various continuous non-Abelian symmetries: (i)  $SU(N)$  (special

unitary) for the orbital, spin-orbital and charge sectors [8, 9, 10]; (ii)  $Sp(N)$  (symplectic) for the spin-charge sector [11], and (iii)  $SO(3)$  (rotational) for the orbital sector [12, 13].

In this paper we present `PointGroupNRG` [14], a Julia [15] code that implements finite point group symmetries in Anderson Hamiltonians. In particular, our code is designed to work with symmetries of the form  $G = U(1)_C \otimes P_O \otimes SU(2)_S$ , where  $U(1)_C$  is the charge symmetry corresponding to particle conservation,  $P_O$  is a simply reducible finite orbital point-group symmetry, and  $SU(2)_S$  represents spin isotropy. These symmetries are appropriate for systems where spin-orbit interactions can be neglected and thus the orbital and spin sectors can be treated separately. Simply reducible point groups include common symmetries such as the cubic crystal point groups and the inversion symmetry. More specifically, the main features of the code are (i) the automatic construction of symmetry-adapted multiplets, (ii) tools to generate fully symmetric Anderson impurity Hamiltonians, and (iii) an iterative diagonalization procedure that exploits the specified symmetries to increase the efficiency and precision of the calculations. The `PointGroupNRG` package is open source. It can be downloaded from [14] alongside a manual, a tutorial, and scripts to build an optional precompiled version. In addition to the singular symmetry-handling features, it also includes modern discretization techniques.

The paper is organized as follows. The first two sections are devoted to those aspects of the procedure that are most specific to our code and the type of symmetries it deals with: Section 2 covers the automatic generation of symmetry-adapted multiplet states and Section 3 deals with the generation of point-group symmetric Hamiltonians. In Section 4 we briefly cover the implementation of the NRG procedure, which follows the approach described in the existing published literature. In Section 5 we showcase the application of `PointGroupNRG` with finite orbital symmetries to a two-impurity system exhibiting RKKY interaction (Section 5.1) and a two-orbital  $E_g$  model (Section 5.2). Finally, Section 6 contains benchmarks that demonstrate the computational advantages of exploiting orbital symmetries with `PointGroupNRG` (Section 6.1) and a performance comparison of `PointGroupNRG` with another code (Section 6.2).

## 2. Symmetry-adapted basis

Our magnetic impurity system has symmetry  $G = U(1)_C \otimes P_O \otimes SU(2)_S$ . To fully exploit it, we choose to work with a symmetry-adapted basis from the outset, so we define symmetry-adapted states

$$|w\rangle = |\Gamma_w, \gamma_w, r_w\rangle, \quad (1)$$

where the quantum numbers  $\Gamma_w$ ,  $\gamma_w$  and  $r_w$  label the irrep, the partner and the outer multiplicity, respectively. Our notation is based on Ref. [8]. Due to the tensor-product structure of the group  $G$ , the irreps can be decomposed as  $\Gamma_w = (N_w, I_w, S_w)$ , where  $N_w$  is the particle number,  $I_w$  is the orbital irrep, and  $S_w$  is the total spin. We label the partners accordingly as  $\gamma_w = (i_w, s_w)$ , where  $i_w$  is the orbital partner label and  $s_w$  is the spin projection (we do not explicitly label charge partners because the irreps  $N_w$  of  $U(1)_C$  are one-dimensional).

The building blocks for constructing the initial basis and updating it at each NRG step are the multiplet states for the impurity and the shells, *i.e.*, the conduction-channel sites [7]. Our `PointGroupNRG` code generates these multiplet states for the impurity and shell subspaces by taking as the only input the relevant Clebsch-Gordan coefficients of the point symmetry group. Here we briefly outline the main steps in the procedure (see also Refs. [16, 17, 18]).

We first construct  $N$ -particle orbital and spin wave functions. Orbital (spin) basis functions have the form  $|\psi\rangle_N = |I_\psi, i_\psi, r_\psi\rangle_N$  ( $|\xi\rangle_N = |S_\xi, s_\xi, r_\xi\rangle_N$ ), where  $I_\psi$  and  $i_\psi$  ( $S_\xi$  and  $s_\xi$ ) are orbital (spin) irrep and partner quantum numbers, respectively, and  $r_\psi$  ( $r_\xi$ ) is the outer multiplicity. The construction is carried out recursively by means of the Clebsch-Gordan series

$$\begin{aligned} |\psi\rangle_N &= \sum_{i_{\psi'}, i_{\psi''}} (I_{\psi'}, i_{\psi'}; I_{\psi''}, i_{\psi''} | I_\psi, i_\psi, r_\psi) |\psi'\rangle_{N-1} \otimes |\psi''\rangle_1, \\ |\xi\rangle_N &= \sum_{s_{\xi'}, s_{\xi''}} (S_{\xi'}, s_{\xi'}; S_{\xi''}, s_{\xi''} | S_\xi, s_\xi, r_\xi) |\xi'\rangle_{N-1} \otimes |\xi''\rangle_1, \end{aligned} \quad (2)$$

where the  $(\dots; \dots | \dots)$  terms are Clebsch-Gordan coefficients.

In order to find the antisymmetric combinations, we implement the apparatus of Young theory [17]. Since the  $N$ -element permutation group  $\mathcal{S}_N$  commutes with the orbital (spin) symmetry group  $P_O$  ( $SU(2)_S$ ), we can further subdivide each subspace of states with quantum numbers  $I_\psi$  and  $i_\psi$  ( $S_\xi$

and  $s_\xi$ ) by introducing permutation irrep and partner quantum numbers,  $A$  and  $a$  ( $B$  and  $b$ ). We do so by going through all the orbital (spin) states and applying the Young symmetrizer  $Y_{A,a}$  ( $Y_{B,b}$ ), which is an operator. The result can be either zero or a wave function of the form

$$\begin{aligned} Y_{A,a} |I_\psi, i_\psi, r_\psi\rangle_N &= |I_\psi, i_\psi, r_{\psi'}; A, a\rangle := |\psi\rangle_N^{A,a} \\ Y_{B,b} |S_\xi, s_\xi, r_\xi\rangle &= |S_\xi, s_\xi, r_{\xi'}; B, b\rangle := |\xi\rangle_N^{B,b}, \end{aligned} \quad (3)$$

where the state  $|\psi\rangle_N^{A,a}$  ( $|\xi\rangle_N^{B,b}$ ) transforms as the  $a$  ( $b$ ) partner of the  $A$  ( $B$ ) irrep of  $\mathcal{S}_N$ . A set of linearly independent states  $|\psi\rangle_N^{A,a}$  ( $|\xi\rangle_N^{B,b}$ ) provides a complete basis of states adapted to the orbital (spin) and permutation symmetries.

Antisymmetric spin-orbital states result from combining orbital and spin states belonging to permutation irreps  $A$  and  $B$  such that the antisymmetric permutation irrep  $\bar{C}$  is contained in the product  $C = A \otimes B$ ,

$$C = A \otimes B = \dots + \bar{n}\bar{C} + \dots, \quad (4)$$

where  $\bar{n}$  is the multiplicity of  $\bar{C}$ , *i.e.*, the number of times  $\bar{C}$  appears in the product  $C$ . Therefore, in order to find the antisymmetric wave functions we do as follows. For each group of quantum numbers  $Q = (N, I_\psi, i_\psi, S_\xi, s_\xi, A, B)$  we construct a basis composed of all tensor product wave functions  $|I_\psi, i_\psi, r_\psi\rangle_N^{A,a} \otimes |S_\xi, s_\xi, r_\xi\rangle_N^{B,b}$  with varying quantum numbers  $a, b, r_\psi$  and  $r_\xi$ . This basis spans a space  $V_C^{(Q)}$  of the representation  $C$  that conserves the quantum numbers  $Q$ . In order to find the subspace belonging to irrep  $\bar{C}$ ,  $V_{\bar{C}}^{(Q)} \subseteq V_C^{(Q)}$ , we first construct a basis of the space  $V_{\bar{C}}$  of all antisymmetric spin-orbital states. The antisymmetric subspace with quantum numbers  $Q$  is the intersection  $V_{\bar{C}}^{(Q)} = V_C^{(Q)} \cap V_{\bar{C}}$ , which we compute numerically to obtain the basis functions

$$|w\rangle = |\Gamma_w, \gamma_w, r_w\rangle = \sum_{r_\psi r_\xi} c_Q(r_\psi, r_\xi; w) |I_w, i_w, r_\psi\rangle_{N_w}^{A,a} \otimes |S_w, s_w, r_\xi\rangle_{N_w}^{B,c}, \quad (5)$$

where the antisymmetric state  $|w\rangle$  is expressed in the spin-orbital tensor product basis of the  $V_C^{(Q)}$  subspace, being  $c_Q(r_\psi, r_\xi; w)$  the coefficients. With a change of basis, we re-express  $|w\rangle$  in the basis of Fock states as

$$|w\rangle = \sum_{\mathbf{a}} c_F(\mathbf{a}; w) \left( \prod_{\alpha_i \in \mathbf{a}} f_{\alpha_i}^\dagger \right) |\Omega\rangle, \quad (6)$$

where  $c_F(\mathbf{a}; w)$  is the coefficient of the  $N_w$  particle Slater determinant state with occupations  $\mathbf{a} = (\alpha_1, \dots, \alpha_{N_w})$ , being  $\alpha_i$  the label for one-particle symmetry-adapted states;  $f_{\alpha_i}^\dagger$  creates a particle in state  $\alpha_i$ , and  $|\Omega\rangle$  represents an empty impurity or shell. Multiplet Fock states  $|w\rangle$  for an impurity and a shell, or for different shells, can then be combined by a regular Clebsch-Gordan series (*i.e.*, regardless of permutation symmetries) in order to iteratively form states along the NRG sequence (see Section 7).

### 3. Construction of a symmetric Hamiltonian

Let us consider a multi-orbital, multi-channel Anderson Hamiltonian

$$\begin{aligned}
\mathcal{H} &= H_{\text{occ}} + H_C + H_{\text{hyb}} + H_{\text{cond}}, \\
H_{\text{occ}} &= \sum_{\alpha} \epsilon_{\alpha} f_{\alpha}^{\dagger} f_{\alpha}, \\
H_C &= \sum_{\alpha_1 \alpha_2 \alpha_3 \alpha_4} U_{\alpha_1 \alpha_2 \alpha_3 \alpha_4} f_{\alpha_1}^{\dagger} f_{\alpha_2}^{\dagger} f_{\alpha_3} f_{\alpha_4}, \\
H_{\text{hyb}} &= \sum_{\alpha \beta} \int_{-D}^D V_{\alpha \beta} [\rho_{\beta}(\epsilon)]^{\frac{1}{2}} (f_{\alpha}^{\dagger} c_{\epsilon \beta} + \text{h.c.}) d\epsilon, \\
H_{\text{cond}} &= \sum_{\beta} \int_{-D}^D c_{\epsilon \beta}^{\dagger} c_{\epsilon \beta} \epsilon d\epsilon.
\end{aligned} \tag{7}$$

In the definitions above, the operators  $f_{\alpha}$  annihilate impurity electrons in the one-particle symmetry-adapted impurity state  $|\alpha\rangle$ ; operators  $c_{\epsilon \beta}$  annihilate conduction electrons with one-particle symmetry quantum numbers  $\beta$  and energy  $\epsilon \in [-D, D]$ , where  $D$  is the half-bandwidth. The Hamiltonian is broken down into the following terms:  $H_{\text{occ}}$  is the occupation term, regulated by the occupation energies  $\epsilon_{\alpha}$ ;  $H_C$  is the screened Coulomb repulsion between electrons, given by the parameters  $U_{\alpha_1 \alpha_2 \alpha_3 \alpha_4}$ ;  $H_{\text{hyb}}$  is the hybridization term, given by the hybridization amplitudes  $V_{\alpha \beta}$  and the density of states (DOS)  $\rho_{\beta}(\epsilon)$  for each channel  $\beta$ , and  $H_{\text{cond}}$  is the conduction term.

We impose symmetry restrictions on the Hamiltonian by applying the selection rule

$$\langle w | \mathcal{H} | w' \rangle \propto \delta_{\Gamma_w, \Gamma_{w'}} \delta_{\gamma_w, \gamma_{w'}}, \tag{8}$$

which makes it explicit that  $\mathcal{H}$  is diagonal in the irrep and partner quantum numbers. This immediately imposes the restrictions for the relevant

parameters and DOS functions in the one-body terms  $H_{\text{occ}}$  and  $H_{\text{hyb}}$ ,

$$\begin{aligned}\epsilon_\alpha &= \epsilon_{r_\alpha}(\Gamma_\alpha), \\ V_{\alpha\beta} &= \delta_{\Gamma_\alpha, \Gamma_\beta} \delta_{\gamma_\alpha \gamma_\beta} V_{r_\alpha r_\beta}(\Gamma_\alpha), \\ \rho_\beta(\epsilon) &= \rho_{r_\beta}(\Gamma_\beta; \epsilon),\end{aligned}\tag{9}$$

where the dependence on  $\Gamma_\alpha$  and  $\Gamma_\beta$  comes only from the orbital part, because  $N_\alpha = N_\beta = 1$  and  $S_\alpha = S_\beta = \frac{1}{2}$ . The independent one-body parameters and functions are thus  $\epsilon_{r_\alpha}(\Gamma_\alpha)$ ,  $V_{r_\alpha r_\beta}(\Gamma_\alpha)$  and  $\rho_{r_\beta}(\Gamma_\beta; \epsilon)$ .

For the two-body Coulomb interaction  $H_C$ , the selection rule given by Eq. 8 must be applied to two-electron symmetry-adapted states

$$|\kappa\rangle = \sum_{\alpha_1 \alpha_2} c(\alpha_1, \alpha_2; \kappa) f_{\alpha_1}^\dagger f_{\alpha_2}^\dagger |\Omega\rangle,\tag{10}$$

where  $c(\alpha_1, \alpha_2; \kappa)$  are the coefficients in Eq. 6. Overall, we have that

$$\begin{aligned}U_{\alpha_1 \alpha_2 \alpha_3 \alpha_4} &= \langle \Omega | f_{\alpha_2} f_{\alpha_1} H_C f_{\alpha_4}^\dagger f_{\alpha_3}^\dagger | \Omega \rangle \\ &= \sum_{\kappa, \kappa'} c^*(\alpha_1, \alpha_2; \kappa) c(\alpha_4, \alpha_3; \kappa') \langle \kappa | H_C | \kappa' \rangle \\ &= \sum_{\kappa, \kappa'} c^*(\alpha_1, \alpha_2; \kappa) c(\alpha_4, \alpha_3; \kappa') \delta_{\Gamma_\kappa \Gamma_{\kappa'}} \delta_{\gamma_\kappa \gamma_{\kappa'}} U_{r_\kappa r_{\kappa'}}(\Gamma_\kappa),\end{aligned}\tag{11}$$

where  $U(\Gamma_\kappa)$  is a real symmetric matrix of real parameters,  $U_{r_\kappa r_{\kappa'}}(\Gamma_\kappa) = U_{r_{\kappa'} r_\kappa}(\Gamma_\kappa)$ . Furthermore, since the orbital basis can be chosen to be real, additional restrictions apply on top of the restrictions derived from the symmetry group  $G$ . In the basis of real orbitals  $\psi_d(\mathbf{r})$ , the Coulomb parameters are

$$U_{d_1 d_2 d_3 d_4} = \int d\mathbf{r} d\mathbf{r}' \psi_{d_1}(\mathbf{r}) \psi_{d_2}(\mathbf{r}') H_C(\mathbf{r}, \mathbf{r}') \psi_{d_3}(\mathbf{r}') \psi_{d_4}(\mathbf{r}).\tag{12}$$

The parameters  $U_{d_1 d_2 d_3 d_4}$  have to reflect the symmetry under the group of permutations in the  $d_i$  indices leaving the integral in Eq. 12 invariant. The restrictions imposed by this permutation symmetry have to be carried over to the symmetry-adapted parameters  $U_{r_\kappa r_{\kappa'}}(\Gamma_\kappa)$ ; this step depends on the orbital basis chosen and on the form of the multiplet states generated by the code.

Importantly, this procedure for constructing  $H_C$  only imposes the finite point-group symmetry to the Coulomb interaction, so it allows us to construct

general non-spherical screened interaction terms  $H_C$  with  $H_C(\mathbf{r}, \mathbf{r}') \neq H_C(|\mathbf{r} - \mathbf{r}'|)$ . For a more comprehensive discussion about Coulomb terms with finite point group symmetries, see Ref. [19].

In summary, we are left with a set of parameters and DOS functions  $\epsilon_{r_\alpha}(\Gamma_\alpha)$ ,  $V_{r_\alpha r_\beta}(\Gamma_\alpha)$ ,  $U_{r_\kappa r'_\kappa}(\Gamma_\kappa)$  and  $\rho_{r_\beta}(\Gamma_\beta; \epsilon)$  that are model specific and can be freely chosen; the implemented construction procedure ensures that the resulting Hamiltonian is hermitic and respects the symmetries of the Coulomb interaction. Our `PointGroupNRG` code takes these parameters as input in order to construct an Anderson Hamiltonian with the desired symmetry.

#### 4. Implementation of the NRG

The first step in the NRG procedure is to discretize the conduction band. We use an interleaved discretization [5, 3], which depends on the discretization parameter  $\Lambda$ , commonly used in NRG calculations [7], and the so-called shift parameter  $z$ . Using a Lanczos algorithm modified for improved numerical robustness [20], the continuous conduction term  $H_{\text{cond}}$  is discretized as

$$\int c_{\epsilon\beta}^\dagger c_{\epsilon\beta} \epsilon d\epsilon \rightarrow \sum_\beta \sum_{n=0}^{\infty} \left[ h_{n\beta}^{(z)} (c_{n\beta}^\dagger c_{n+1,\beta} + \text{h.c.}) + e_{n\beta}^{(z)} c_{n\beta}^\dagger c_{n\beta} \right], \quad (13)$$

where  $c_{n\beta}^\dagger$  ( $c_{n\beta}$ ) creates (annihilates) an electron at the  $n$ -th conduction shell,  $h_{n\beta}^{(z)}$  are the hopping factors, and  $e_{n\beta}^{(z)}$  are the on-site energies. As in Eq. 9, symmetry restricts the hopping and on-site terms to a minimal set,

$$\begin{aligned} h_{n\beta}^{(z)} &= h_{nr_\beta}^{(z)}(\Gamma_\beta), \\ e_{n\beta}^{(z)} &= e_{nr_\beta}^{(z)}(\Gamma_\beta). \end{aligned} \quad (14)$$

Once the bands are discretized, we write a series of Hamiltonians

$$H_N = \Lambda^{(N-1)/2} \left[ \sum_{n=0}^{N-1} h_{n\beta}^{(z)} (c_{n,\beta}^\dagger c_{n+1,\beta} + \text{h.c.}) + \sum_{n=0}^N e_{n\beta}^{(z)} c_{n\beta}^\dagger c_{n\beta} + H_0 \right], \quad (15)$$

where  $H_0 = H_{\text{occ}} + H_C + H_{\text{hyb}}$ . This sequence of Hamiltonians  $H_N$  is iteratively constructed, diagonalized and truncated following the symmetry-adapted procedure described in Ref. [8] (see Appendix A). Using symmetry we are able to effectively reduce the Hilbert space by directly working with multiplets with quantum numbers  $(\Gamma_w, r_w)$ , each representing a number of



states equal to  $\dim(I_w)(2S_w + 1)$ , where  $\dim(I_w)$  is the dimension of the  $I_w$  orbital irrep of the multiplet. Moreover, the block-diagonal structure of the Hamiltonian in the indices  $\Gamma_w$  allows for an efficient block-wise diagonalization.

The code is optimized so that the overhead from the implementation of symmetry in the block-diagonalization procedure is minimal. By efficiently managing the reduced matrices and using pre-computed Clebsch-Gordan factors (see Appendix A), we are able to reduce the time spent outside of the matrix diagonalization function to less than half of the total computation time for most calculations. Importantly, the relative weight of the diagonalization grows with the size of the Hilbert space, so in demanding calculations we obtain all the advantages of block-diagonalization at a very little computational cost.

## 5. Applications

In this section we apply the `PointGroupNRG` code to two impurity models. First we use it to solve a two-impurity model with RKKY interaction [21, 22, 23], which serves to illustrate the symmetry-adapted approach with a simple point group and it also incorporates a non-constant DOS. Then we focus on a two-orbital, two-channel  $E_g$  model with cubic symmetry, which we compare with an approximate Dworin-Narath model with continuous  $SU(2)_O$  orbital symmetry.

### 5.1. Two-impurity model with RKKY interaction

The model consists of two identical  $s$ -shell Anderson impurities with a separation vector  $\mathbf{R}$  placed in flat band of electrons with linear dispersion relation  $\epsilon = v_F(k - k_F)$  measured from the Fermi level with  $v_F = D/k_F$ . The system is symmetric under inversion with respect to the middle point between the impurities, so we work with the  $C_i$  point group. The symmetry-adapted orbitals are even (+) and odd (-) combinations of the impurity  $s$  orbitals  $\psi_1(\mathbf{r}) = \psi(\mathbf{r} + \mathbf{R}/2)$  and  $\psi_2(\mathbf{r}) = \psi(\mathbf{r} - \mathbf{R}/2)$ ,

$$\psi_{\pm}(\mathbf{r}) = \frac{1}{\sqrt{2}}[\psi_1(\mathbf{r}) \pm \psi_2(\mathbf{r})], \quad (16)$$

which belong to the irreducible representations  $A_g$  (even) and  $A_u$  (odd) of  $C_i$ , respectively. It is worth noting that other group choices featuring one-dimensional irreducible representations  $A$  and  $B$  equivalent to even and odd,

*i.e.*, fulfilling  $A \otimes A = A$ ,  $A \otimes B = B$  and  $B \otimes B = A$ , are also valid in this case. In general, what determines the application of symmetry in the model is not the group and its group elements (symmetry operations), but the irreducible representations appearing in the system and their products.

Using the orbitals  $\psi_{\pm}$ , `PointGroupNRG` generates the multiplet states, which are shown in Table 1 for up to  $N = 2$  particles. This information allows us to define the symmetry-adapted parameters of the Hamiltonian. Starting with the impurity term  $H_{\text{imp}}$ , we assign equal occupation energies to the orbitals,

$$\epsilon_1(\Gamma_1) = \epsilon_1(\Gamma_2) = \epsilon_{\pm} = \epsilon. \quad (17)$$

To determine the Coulomb parameters, we assume that the only non-vanishing Coulomb integral (Eq. 12) is the on-site repulsion  $U := U_{1111} = U_{2222}$  in each of the impurities. Then, taking into account the orbital part of the two-particle multiplets and Eq. 16, it can be shown, by inverting Eq. 11, that the symmetry-adapted parameters are

$$\mathbf{U}(\Gamma_3) = \frac{U}{2} \begin{pmatrix} 1 & 1 \\ 1 & 1 \end{pmatrix}, \quad U_{11}(\Gamma_4) = U, \quad U_{11}(\Gamma_5) = 0. \quad (18)$$

$\Gamma = (N, I, S)$	$r$	Orbital part	Spin part
$\Gamma_1 = (1, A_g, \frac{1}{2})$	1	$\psi_+$	$\uparrow, \downarrow$
$\Gamma_2 = (1, A_u, \frac{1}{2})$	1	$\psi_-$	$\uparrow, \downarrow$
$\Gamma_3 = (2, A_g, 0)$	1	$\psi_- \psi_-$	$\frac{1}{\sqrt{2}}(\uparrow\downarrow - \downarrow\uparrow)$
	2	$\psi_+ \psi_+$	$\frac{1}{\sqrt{2}}(\uparrow\downarrow - \downarrow\uparrow)$
$\Gamma_4 = (2, A_u, 0)$	1	$\frac{1}{\sqrt{2}}(\psi_+ \psi_- + \psi_- \psi_+)$	$\frac{1}{\sqrt{2}}(\uparrow\downarrow - \downarrow\uparrow)$
$\Gamma_5 = (2, A_u, 1)$	1	$\frac{1}{\sqrt{2}}(\psi_+ \psi_- - \psi_- \psi_+)$	$\uparrow\uparrow, \frac{1}{\sqrt{2}}(\uparrow\downarrow + \downarrow\uparrow), \downarrow\downarrow$

Table 1: Orbital and spin parts of the one-particle and two-particle multiplet states of the two impurities. Following the procedure described in Section 2, two-particle orbital states are obtained by combining  $\psi_+ \psi_+$ ,  $\psi_+ \psi_-$ ,  $\psi_- \psi_+$  and  $\psi_- \psi_-$  so that the resulting state (i) has a definite orbital symmetry  $A_g$  or  $A_u$ , and (ii) is symmetrized with respect to particle permutations. Permutation-symmetric (-antisymmetric) orbital states are then combined with permutation-antisymmetric (-symmetric) spin states to obtain the full permutation-antisymmetric multiplet states.

The hybridizations between the even and odd orbitals and the electron

bath are given by [24]

$$\Delta_{\pm}(\epsilon) := \pi \rho_{\pm}(\epsilon) V_{\pm}^2 = \Delta_0 \left( 1 \pm \frac{\sin k(\epsilon)R}{k(\epsilon)R} \right), \quad (19)$$

where  $\Delta_0$  is the hybridization at  $kR \rightarrow \infty$ ,  $k(\epsilon) = \epsilon/v_F + k_F$  is given by the dispersion relation, and  $\rho_{\pm}(\epsilon)$  and  $V_{\pm}$  are defined by absorbing the energy-dependence of  $\Gamma_{\pm}(\epsilon)$  into  $\rho_{\pm}(\epsilon)$  and requiring that

$$\int_{-D}^D d\epsilon \rho_{\pm}(\epsilon) = 1. \quad (20)$$

Thus,  $\rho_{\pm}(\epsilon)$  and  $V_{\pm}$  can be regarded as the effective density of states and hybridization amplitude for the corresponding channel, respectively. Following their definition, these are given by

$$\begin{aligned} \rho_{\pm}(\epsilon) &= \frac{1 \pm \frac{\sin k(\epsilon)R}{k(\epsilon)R}}{\int_{-D}^D d\epsilon \left( 1 \pm \frac{\sin k(\epsilon)R}{k(\epsilon)R} \right)}, \\ V_{\pm} &= \left[ \frac{\Delta_0}{\pi} \int_{-D}^D d\epsilon \left( 1 \pm \frac{\sin k(\epsilon)R}{k(\epsilon)R} \right) \right]^{\frac{1}{2}}. \end{aligned} \quad (21)$$

The symmetry-adapted expressions for these parameters are

$$\rho_1(\Gamma_1; \epsilon) = \rho_+(\epsilon), \quad \rho_1(\Gamma_2; \epsilon) = \rho_-(\epsilon), \quad V_1(\Gamma_1) = V_+, \quad V_1(\Gamma_2) = V_-. \quad (22)$$

To show the competition between the RKKY interaction and the Kondo effect, we have computed the entropy  $S$  and magnetic susceptibility  $\chi$  as a function of temperature for various inter-impurity distances, which result in different values of  $k_F R$ . For all the calculations we used a discretization parameter  $\Lambda = 10$  and a cutoff of 1300 multiplets. The results are given in Fig. 1. For  $k_F R = \frac{\pi}{2}$ , the band-induced RKKY interaction  $I_{\text{RKKY}}^{[\pi/2]}$  is ferromagnetic and larger than the Kondo energy scale,  $I_{\text{RKKY}}^{[\pi/2]} \gg k_B T_K^{[\pi/2]}$ , which results in the development of a ferromagnetically coupled ground state at  $k_B T \approx 10^{-5} D$ . Since  $\Delta_+ > \Delta_-$ , this RKKY spin-1 local moment is partially screened first by the even channel at  $k_B T \approx 10^{-10} D$ , and then completely screened by the odd channel at  $k_B T \approx 10^{-20} D$ . For  $k_F R \rightarrow \infty$ , the hybridizations are constant and equal,  $\Delta_{\pm} = \Delta_0$ , so there is no RKKY interaction and the spin- $\frac{1}{2}$  impurity local moments are separately screened

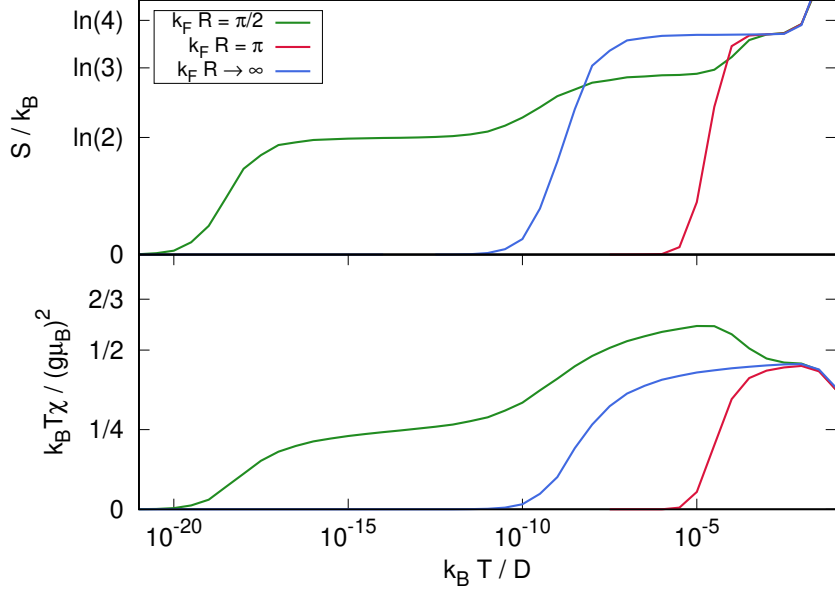


Figure 1: Entropy  $S/k_B$  and magnetic susceptibility  $k_B T \chi / (g \mu_B)^2$  curves as a function of temperature for the two-impurity system with RKKY interaction, where  $k_B$  is the Boltzmann factor,  $g = 2$  is the Landé factor, and  $\mu_B$  is Bohr's magneton. The calculations are performed with fixed  $\epsilon = -0.1$ ,  $U = 0.2$  and  $\Delta_0 = 0.005$ , all in units of the half-bandwidth  $D$ , and varying values of  $k_F R = \frac{\pi}{2}$ ,  $\pi$  and  $\infty$ . The values marked in the  $y$  axis in the top (bottom) graph correspond to fixed points of the Hamiltonian:  $\ln(4)$  and  $1/2$  correspond to the double local moment regime where the impurities behave as independent spin- $\frac{1}{2}$  local moments,  $\ln(3)$  and  $3/2$  correspond to the RKKY fixed point where the impurity spins are ferromagnetically coupled, and  $\ln(2)$  and  $1/4$  correspond to the partially screened screened fixed point where the RKKY-coupled spin-1 is partially screened by the even channel (note that  $\Delta_+ > \Delta_-$ ).

at an energy scale  $k_B T_K^{[\infty]} \approx 10^{-8} D$ . For  $k_F R = \pi$ , the RKKY interaction is antiferromagnetic and larger in magnitude than the Kondo scale,  $-I_{\text{RKKY}}^{[\pi]} \gg k_B T_K^{[\pi]}$ , which results in the formation of an antiferromagnetic ground state at an energy scale  $I_{\text{RKKY}}^{[\pi]} \approx 10^{-5} D$ . The results obtained here with the Anderson model agree with the perturbative analysis in Ref. [25] and with the NRG results obtained in Ref. [26] using a Kondo model for the same system.

### 5.2. Two-orbital $E_g$ model

We now investigate a model consisting of two orbitals belonging to the irreducible representation  $E_g$  of the cubic point group  $O_h$ , each one connected

to a channel of the same symmetry. This model can be regarded as a transition metal impurity with the outer  $d$  shell degeneracy split by a crystal field with cubic symmetry  $O_h$  into a three-fold degenerate  $T_{2g}$  upper level and a two-fold degenerate  $E_g$  lower level, where the energy difference between the two of them is sufficiently large to discard the  $T_{2g}$  subspace altogether.

For the orbital part, we use the basis functions and Clebsch-Gordan coefficients found in the tables by Altmann and Herzig [27]. The orbital basis functions are

$$\begin{aligned}\psi_1(\mathbf{r}) &= \frac{1}{\sqrt{2}}[\psi_a(\mathbf{r}) - i\psi_b(\mathbf{r})] \\ \psi_2(\mathbf{r}) &= \frac{1}{\sqrt{2}}[\psi_a(\mathbf{r}) + i\psi_b(\mathbf{r})]\end{aligned}\tag{23}$$

where  $\psi_a(\mathbf{r}) = R(r)Y_2^0(\theta, \varphi)$  and  $\psi_b(\mathbf{r}) = R(r)[Y_2^2(\theta, \varphi) + Y_2^{-2}(\theta, \varphi)]/\sqrt{2}$  are real harmonics with a radial term  $R(r)$ .

$\Gamma = (N, I, S)$	$T$	$i$	Orbital part
$\Gamma_1 = (1, E_g, \frac{1}{2})$	$\frac{1}{2}$	1	$\psi_1$
		2	$\psi_2$
$\Gamma_2 = (2, E_g, 0)$	1	1	$\psi_2\psi_2$
		2	$\psi_1\psi_1$
$\Gamma_3 = (2, A_{1g}, 0)$	1	1	$\frac{1}{\sqrt{2}}(\psi_1\psi_2 + \psi_2\psi_1)$
$\Gamma_4 = (2, A_{2g}, 1)$	0	1	$\frac{1}{\sqrt{2}}(\psi_1\psi_2 - \psi_2\psi_1)$

Table 2: Orbital structure of the one-particle and two-particle multiplet states of the  $E_g$  impurity. Column  $\Gamma$  specifies the irrep,  $T$  is the orbital isospin, and  $i$  is the orbital partner label.

We now have to find the independent parameters of the Hamiltonian. In this case, the only one-body irrep is  $\Gamma_1 = (1, E_g, \frac{1}{2})$ , and the two-body irreducible representations are  $\Gamma_2 = (2, E_g, 0)$ ,  $\Gamma_3 = (2, A_{1g}, 0)$  and  $\Gamma_4 = (2, A_{2g}, 1)$ ; we use these irreducible representations to label the corresponding multiplets. As in Section 5.1, we use the orbital part of multiplet states provided by `PointGroupNRG` and given in Table 2 to obtain the independent parameters

$$\epsilon := \epsilon_1(\Gamma_1), \quad V := V_{11}(\Gamma_1), \quad U_2 := U_{11}(\Gamma_2), \quad U_3 := U_{11}(\Gamma_3), \quad U_4 := U_{11}(\Gamma_4).\tag{24}$$

We can relate our independent Coulomb parameters to the usual Coulomb integrals obtained in the basis of real orbitals  $\psi_a(\mathbf{r})$  and  $\psi_b(\mathbf{r})$ . The only

non-vanishing terms are the intra-orbital repulsion  $U := U_{aaaa}$ , the inter-orbital repulsion  $U' := U_{abba}$ , the exchange  $J := U_{abab}$ , and the pair-hopping  $J' := U_{aabb}$  (note that  $a$  and  $b$  can be interchanged). Using Eq. 23 and the expressions of the multiplet states in Table 2, we obtain the general expressions shown in Table 3. If (i) we impose the physical condition  $J = J'$  that results from the permutation symmetry in the basis of real orbitals and (ii) we use the selection rule that forbids transitions between different partners of irrep  $\Gamma_2$ , we obtain an additional set of equivalent restrictions, namely,  $2U_2 = U_3 + U_4$  and  $U' = U - 2J$ . For an  $E_g$  subspace, these restrictions are the same as for Coulomb interactions with cubic and full rotational symmetries [28, 19]. This leaves us with two independent Coulomb parameters for the  $O_h$ -symmetric system, as shown in Table 3.

	General	$O_h, J' = J$	$SU(2)_O, J' = 0$
$U_2$	$\frac{1}{2}(U + U' + J - J')$	$U + J$	$U$
$U_3$	$U + J'$	$U - J$	$U$
$U_4$	$U' - J$	$U - 3J$	$U - 2J$

Table 3: Relation between symmetry-adapted Coulomb parameters and the usual Coulomb integrals for the general case, *i.e.*, before applying orbital symmetries and the restrictions on  $J'$ , for the  $O_h$ -symmetric model and for the  $SU(2)_O$ -symmetric model.

As a first step, let us consider the application of continuous symmetries to this system. For a full orbital symmetry  $SU(2)_O$  we need to set  $U_2 = U_3$  because the orbital irreps  $\Gamma_1$  and  $\Gamma_2$  irreps have the same orbital isospin  $T = 1$  (see Table 2). This condition is fulfilled in our  $O_h$ -symmetric model by setting  $J = 0$ , which removes the Hund physics from the system. An alternative is to ignore the pair-hopping terms by setting  $J' = 0$  and  $J \neq J'$ ; this choice gives us the Dworin-Narath Hamiltonian [29, 30] used in a previous work for a similar two-orbital  $E$  model [31]. It has the advantage of exhibiting Hund physics while preserving  $SU(2)_O$  symmetry, but it must be emphasized that it is only an approximation, because by choosing  $J' = 0$  we break the permutation symmetry of the Coulomb integrals in the basis of real orbitals.

In order to examine the numerical difference between the  $O_h$ -symmetric model and the  $SU(2)_O$ -symmetric model, we perform entropy  $S$  and magnetic susceptibility  $\chi$  calculations for both systems with varying  $J$ , fixed  $\epsilon = -U = -0.1$ , and a constant hybridization  $\Delta = \rho\pi V^2 = 0.002$  and DOS  $\rho = 1/2$ , all in units of the half-bandwidth  $D$ . The parameters are chosen so as to showcase the Hund physics of the systems: for  $J > 0$  the  $S = 1$

states belonging to irrep  $\Gamma_4$  have the lowest energy; for  $J = 0$  both models are equivalent and they possess  $SU(4)_{SO}$  spin-orbital symmetry. We set the discretization parameter to  $\Lambda = 10$  and we average over the results obtained with  $z = 0$  and  $z = 1/2$ . At each iteration we keep a minimum of 600 multiplets, which amounts to approximately 1500 states on average. In Fig. 5.2 we show the calculated impurity contributions to the entropy and magnetic susceptibility as a function of temperature. For both systems, we observe that by increasing  $J$  the system gets closer to the spin-1 local moment fixed point, where  $k_B T \chi / (g \mu_B)^2 = 2/3$ , and  $S/k_B = \ln(3)$ , before finally reaching the low-temperature strong coupling fixed point where  $\chi = S = 0$ . This leads to a lower Kondo temperature, as expected from previous studies [30]. Comparing the curves of the two models for the same parameter choices, we see that the  $O_h$ -symmetric model has lower Kondo temperatures than the  $SU(2)_O$ -symmetric model. This is a result of the difference in the Coulomb parameters (see Table 3), which increases the energy gap between the  $\Gamma_4$  ground multiplet and the multiplets  $\Gamma_1$  and  $\Gamma_5 = (3, E_g, \frac{1}{2})$  in the  $O_h$  case as compared to the  $SU(2)_O$  case; these are the multiplets that contribute to the Kondo coupling mechanism up to second order in perturbation theory. In conclusion, having a larger energy gap means that the antiferromagnetic coupling is weaker [32].

## 6. Benchmarks

In this section we provide two types of performance benchmarks for the code. First we measure the improvements in speed and memory efficiency obtained when using `PointGroupNRG` with orbital symmetries. Then we compare the performance of `PointGroupNRG` versus `NRGLjubljana` [33], a widely used [34, 35, 36, 37] open-source NRG code. All calculations are performed on a computer with an Intel(R) Core(TM) i7-10750H processor and 16GB of RAM. For the benchmark, the `PointGroupNRG` code has been compiled and saved into a sysimage using `PackageCompiler.jl`, which removes the latency due to package loading and function compilation [38]. Scripts to perform this precompilation are provided with the code. As performance indicators, we use the elapsed time and maximum resident set size (max. RSS) for each serial run with an increasing number of multiplet cutoffs. The max. RSS is a measure of the peak memory usage of the process. For all calculations, the number of NRG iterations is 42 and the discretization parameter is  $\Lambda = 3$ .

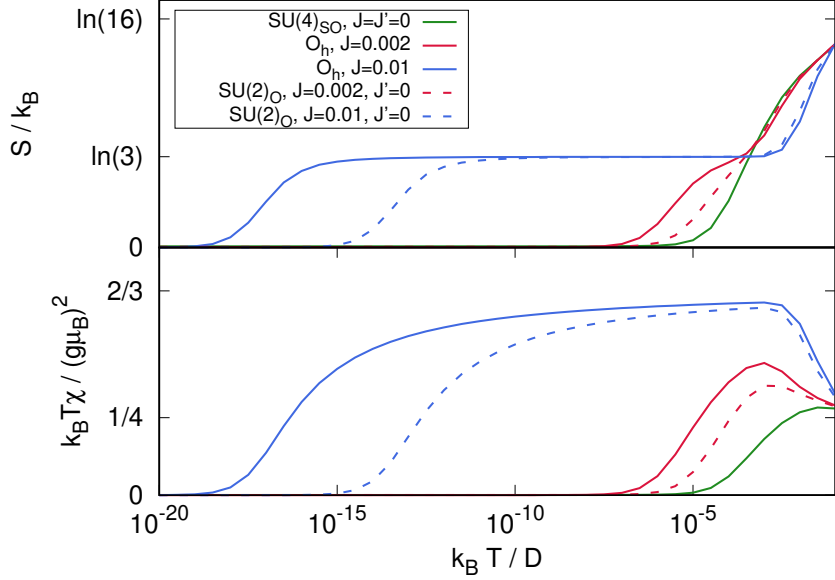


Figure 2: Entropy and magnetic susceptibility curves as a function of temperature for the two-orbital  $E_g$  system for fixed  $\epsilon = -U = -0.1$  and  $\Delta = 0.002$  with varying values of  $J = 0, 0.002$  and  $0.01$ . The values marked in the  $y$  axis in the top (bottom) graph correspond to fixed points of the Hamiltonian:  $\ln(16)$  and  $1/4$  correspond to the free orbital regime where all the impurity states are degenerate,  $\ln(3)$  and  $3/2$  correspond to the fixed point where the impurity behaves as a local moment with spin  $S = 1$ .

### 6.1. Performance improvement with symmetry

To quantify the effect of considering symmetries by the methods described in this work, we measure the total computation time and the peak memory usage in calculations for increasingly larger orbital point groups: the identity point group  $I$  (no orbital symmetry), the inversion group  $C_i$  with one  $A_{1g}$  orbital and one  $A_{1u}$  orbital (as in Sec. 5.1), and the cubic group  $O_h$  with two  $E_g$  orbitals (see Sec. 5.2). We apply them to the same model consisting of two orbitals, with a corresponding impurity Hamiltonian  $H_{\text{imp}} = H_{\text{occ}} + H_C = 0$ , and two channels, each coupled to one orbital with an equal hybridization  $\Delta = 0.1D$ . The results are shown in Fig. 3 for various multiplet cutoffs.

For a given multiplet cutoff, it can be seen that the peak memory usage is reduced as the exploited symmetry becomes larger. Regarding speed, an improvement results from using  $C_i$  or  $O_h$  over  $I$ , but no appreciable difference results from choosing  $O_h$  over  $C_i$ . Overall, these results meet two expected behaviors: (i) the diagonalization is faster because, by applying a



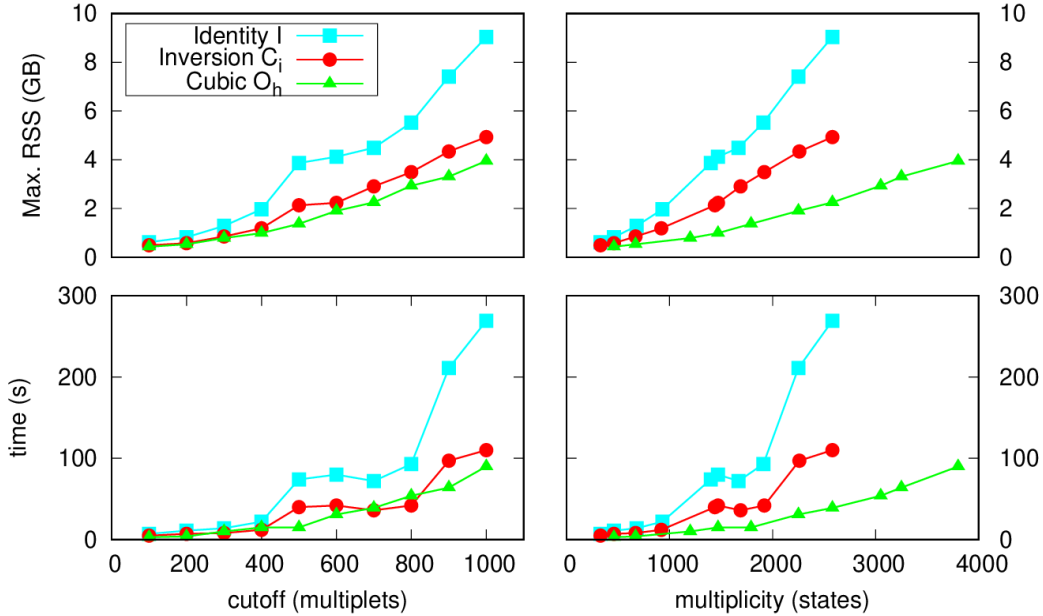


Figure 3: Time (bottom panels) and maximum resident set size (top panels) for the two-impurity, two-channel Anderson Hamiltonian for various multiplet cutoffs. The results are shown as a function of the cutoff (left panels) and as a function of the average number of states represented at the last two steps for the corresponding cutoff (right panels).

larger orbital symmetries, the (already block-diagonal) reduced matrix  $H_N$  for each NRG iteration  $N$  is split into a larger number of blocks, each block corresponding to an irreducible representation  $\Gamma_u$  of the point group  $P$ ; (ii) less memory is needed when updating the Hamiltonian at each step, as the newly added conduction shell subspace is represented by fewer multiplets.

If we compare the results as a function of the multiplicity (Fig. 3 right column), *i.e.* the number of states represented by the multiplets kept at each iteration, the advantage of exploiting  $O_h$  over  $C_i$  becomes apparent. Compared to the results obtained when comparing runs with equal multiplet cutoffs (Fig. 3 left column), the time and memory gains are explained by the fact that the number of states represented by each of the multiplets grows by a factor equal to the dimension  $\dim(\Gamma_u)$  of the irreducible representation  $\Gamma_u$  to which the multiplet belongs. Therefore, the same physical cutoff can be treated in a more compact and efficient manner when the irreducible representations have a larger dimension. In this case, with  $O_h$  we have  $E_g$  with  $\dim(E_g) = 2$ , which explains the difference with respect to the  $I$  and  $C_i$

cases, where all the orbital irreducible representations are one-dimensional.

### 6.2. Comparison with another code

As a performance standard we choose `NRGLjubljana`[33, 13]. Part of `NRGLjubljana` is written in Mathematica, which is used for the preparation of the basis, the operators and the initial Hamiltonian, and part in C++, where the numerically intensive sections of the procedure are performed.

For the comparison of `PointGroupNRG` with `NRGLjubljana`, we have performed calculations for a single-orbital, single-channel model (M1) and a model with two orbitals and channels (M2). The model has  $H_{\text{imp}} = 0$  and a hybridization  $\Delta = 0.1D$  for every channel. With both codes we use the symmetry  $U(1)_C \otimes SU(2)_S$ , which is achieved in `PointGroupNRG` by setting the orbital symmetry to be the identity group and in `NRGLjubljana` by choosing the tag `syntype=QS`. The results are shown in Fig. 4.

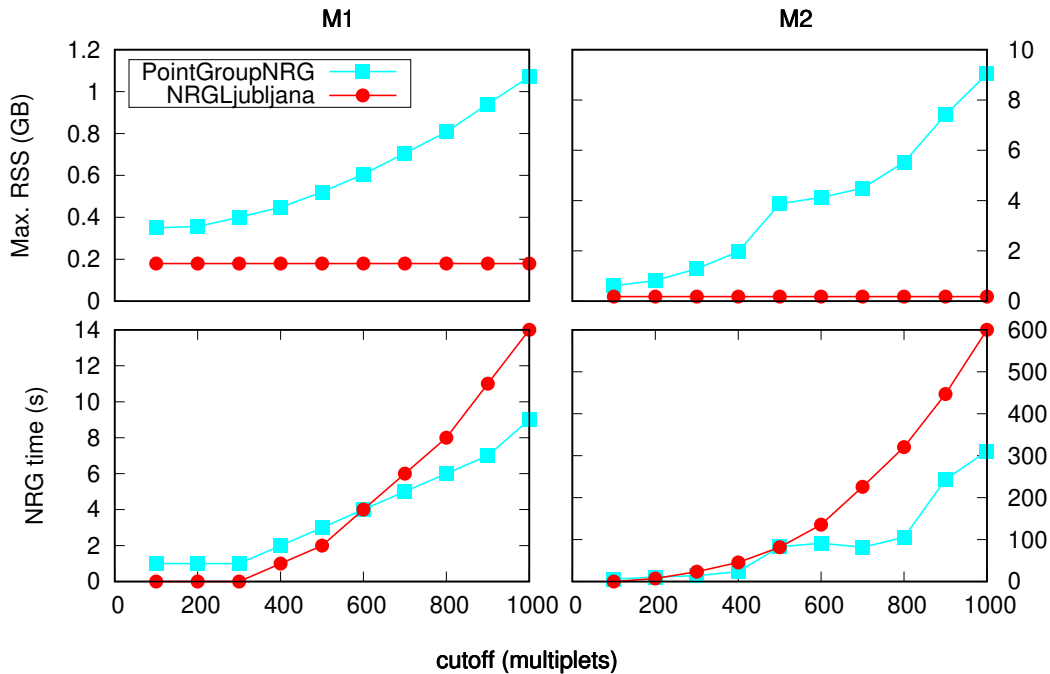


Figure 4: NRG calculation time (bottom panels) and maximum resident set size (top panels) for the one-orbital, one-channel model (left panels) and the two-orbital, two-channel model (right panels) for various multiplet cutoffs.

Peak memory (max. RSS) results show that `PointGroupNRG` requires significantly more memory than `NRGLjubljana`. The larger max. RSS is

partially attributed to the memory management of the Julia language [39]. The computation time is of the same order of magnitude overall for both codes with the chosen multiplet cutoffs, with `PointGroupNRG` being faster for large cutoffs. With the addition of symmetry, the speed is further improved and the memory demands are diminished, as shown in Fig. 3.

## 7. Conclusions

We have presented our Julia code, `PointGroupNRG`, which provides a simple and flexible framework for constructing and solving magnetic impurity models with finite point group symmetries. By exploiting the existing orbital symmetries, it allows efficient and precise NRG calculations without the need to work with approximate models with continuous symmetry. We have obtained results using Anderson impurity Hamiltonians with up to two channels. Models of this kind can be used for transition metal impurities in crystalline environments. This includes, for example, adatoms on metallic surfaces [40], impurities in nanotubes [41], and impurities in metallic chains [42, 31, 43], and it can also be applied to several quantum dot systems [44, 45, 46]. We have showcased the `PointGroupNRG` code by applying it to a parity-symmetric two-impurity model with energy-dependent DOS exhibiting RKKY interaction and to a two-orbital  $E_g$  model with cubic  $O_h$  symmetry.

The `PointGroupNRG` code can also be extended to cover different models. One such extension would be to include spin-orbit coupling, which can be achieved by using a double group instead of the orbital point group. This would make it possible to apply the code to  $f$ -shell impurity systems.

As shown by the performance benchmarks, the code allows for fast calculations for arbitrary models with any point group symmetry. We have also demonstrated the advantage of using orbital symmetries, which results in faster and more memory-efficient calculations.

## Acknowledgements

We acknowledge grants No. IT-1527-22, funded by the Department of Education, Universities and Research of the Basque Government, No. PID2019-103910GB-I00 funded by MCIN/AEI, 10.13039/501100011033/, and No. PRE2020-092046 funded by the Ministry of Education of Spain.

## Appendix A.

The core of the symmetry-adapted approach in terms of iterating through NRG steps is the reduced matrix representation, which relies on the Wigner-Eckart theorem. The latter states that for an operator  $\mathcal{O}_a$  that transforms as the  $\gamma_a$  partner of irrep  $\Gamma_a$ , its matrix elements in a basis of symmetry-adapted states  $|u\rangle, |v\rangle$  fulfill

$$\langle u | \mathcal{O}_a | v \rangle = \langle m_u | | \mathcal{O}_{m_a} | | m_v \rangle (\Gamma_a, \gamma_a; \Gamma_v, \gamma_v | \Gamma_u, \gamma_u, r_u)^*, \quad (.1)$$

where  $\langle m_u | | \mathcal{O}_{m_a} | | m_v \rangle$  is a reduced matrix element that depends only on the multiplet quantum numbers  $m_u = (\Gamma_u, r_u)$  and  $m_v = (\Gamma_v, r_v)$ .

When diagonalizing the Hamiltonian at each step, the reduced representation provides a two-fold advantage. On the one hand, since the Hamiltonians  $H_N$  are fully symmetric with respect to  $G$ , the matrix elements are block-diagonal in the irreps,  $\langle m_u | | H_N | | m_v \rangle \propto \delta_{\Gamma_u, \Gamma_v}$ . On the other hand, each of the blocks is smaller by a factor of  $\dim(\Gamma_u)$  than the blocks that would result from the full matrix. This makes the calculations faster and, since the degeneracies are treated exactly, also more precise. Our `PointGroupNRG` code implements the general expressions given in Ref. [8] adapted to the case of a finite symmetry group  $G$ . Below we give the main equations.

In order to update the Hamiltonian, we first decompose the reduced matrix elements as

$$\langle m_u | | H_N | | m_v \rangle_{(N)} = \delta_{m_u, m_v} (\Lambda^{1/2} E_{m_i}^{(N)} + \langle m_\mu | | \mathcal{E}_N | | m_\mu \rangle) + \langle m_u | | \tau_N | | m_v \rangle_{(N)}. \quad (.2)$$

The diagonal elements are given by  $\Lambda^{1/2} E_{m_i}^{(N)}$ , the rescaled eigenenergy of the  $m_i$  multiplet of step  $N$ , and the rescaled shell occupation energy  $\langle m_\mu | | \mathcal{E}_N | | m_\mu \rangle$ , where

$$\mathcal{E}_N = \Lambda^{\frac{N}{2}} \sum_{\beta} e_{N\tau\beta}^{(z)} c_{N\beta}^\dagger c_{N\beta} \quad (.3)$$

and  $m_\mu$  and  $m_\nu$  are multiplets of the newly added shell. The non-diagonal terms are given by the matrix elements of the hopping operator  $\tau_N$ , which is defined as

$$\tau_N = \Lambda^{\frac{N-1}{2}} \sum_{\beta} h_{N-1, \tau\beta}^{(z)} (\Gamma_\beta) c_{N-1, \beta}^\dagger c_{N\beta} + \text{h.c.} \quad (.4)$$

The multiplets to be diagonalized in step  $n$  are obtained by combining shell multiplets, which contain only electrons in the newly added shell, and

block multiplets, which combine electrons from all the previous shells. The notation is as follows. For a  $N$ -th step matrix element, marked with a subscript  $N$ , the multiplets  $m_u$  ( $m_v$ ) to be diagonalized are obtained by combining block multiplets  $m_i$  ( $m_j$ ) with shell multiplets  $m_\mu$  ( $m_\nu$ ). Following this convention, the hopping matrix element is constructed as

$$\begin{aligned} \langle m_u || \tau_N || m_v \rangle_{(N)} &= \delta_{\Gamma_u, \Gamma_v} (-1)^{N_\mu} \sum_{m_\beta} h_{Nr_\beta}^{(z)}(\Gamma_\beta) \langle m_\nu || c_{Nm_\beta}^\dagger || m_\mu \rangle_{(N)}^* \\ &\times \langle m_i || c_{N-1, m_\beta}^\dagger || m_j \rangle_{(N)} D(\Gamma_u, \Gamma_v, \Gamma_i, \Gamma_j, \Gamma_\mu, \Gamma_\nu, \Gamma_a) + \text{h.c.}, \end{aligned} \quad (.5)$$

Here  $N_\mu$  is the number of particles in the  $m_\mu$  multiplet and  $\langle m_\nu || c_{Nm_\beta}^\dagger || m_\mu \rangle_{(N)}$  is a reduced matrix element involving only shell degrees of freedom and therefore independent of the step  $N$ , so it is computed once and used at every step. The reduced matrix element involving the block multiplets  $m_i$  and  $m_j$  is computed with the information from the previous step: if we denote the multiplets of the diagonal basis of any given iteration as  $m_{u'}$  ( $m_{v'}$ ), then the matrix elements between  $m_i$  and  $m_j$  are just  $\langle m_i || c_{N-1, m_\beta}^\dagger || m_j \rangle_{(N)} = \langle m_{u'} || c_{N-1, m_\beta}^\dagger || m_{v'} \rangle_{(N-1)}$ . We decompose the block matrix elements as

$$\begin{aligned} \langle m_{u'} || c_{N-1, m_\beta}^\dagger || m_{v'} \rangle_{(N-1)} &= \sum_{r_u, r_v} [U_{r_u, r'_u}^{(N-1)}(\Gamma_u)]^* U_{r_v, r'_v}^{(N-1)}(\Gamma_v) \delta_{m_i, m_j} \\ &\times \langle m_\mu || c_{N-1, m_\beta}^\dagger || m_\nu \rangle_{(N-1)} K(\Gamma_u, \Gamma_v, \Gamma_i, \Gamma_\mu, \Gamma_\nu, \Gamma_a), \end{aligned} \quad (.6)$$

where  $U^{(N-1)}(\Gamma_u)$  is the unitary matrix that diagonalizes the subspace of irrep  $\Gamma_u$  in step  $N-1$ . The coefficients  $D$  and  $K$  in Eqs. .5 and .6 are summations over Clebsch-Gordan indices,

$$\begin{aligned} D(\Gamma_u, \Gamma_v, \Gamma_i, \Gamma_j, \Gamma_\mu, \Gamma_\nu, \Gamma_a) &= \sum_{\gamma_\mu, \gamma_i} \sum_{\gamma_\nu, \gamma_j} \sum_{\gamma_a} (\Gamma_\nu, \gamma_\nu; \Gamma_j, \gamma_j | \Gamma_v, \gamma_v, r_v) \\ &\times (\Gamma_\mu, \gamma_\mu; \Gamma_i, \gamma_i | \Gamma_u, \gamma_u, r_u)^* (\Gamma_a, \gamma_a; \Gamma_\mu, \gamma_\mu | \Gamma_\nu, \gamma_\nu, r_\nu) (\Gamma_a, \gamma_a; \Gamma_\mu, \gamma_\mu | \Gamma_\nu, \gamma_\nu, r_\nu)^*, \end{aligned} \quad (.7)$$

$$\begin{aligned} K(\Gamma_u, \Gamma_v, \Gamma_i, \Gamma_\mu, \Gamma_\nu, \Gamma_a) &= \frac{1}{\dim(\Gamma_u)} \sum_{\gamma_a} \sum_{\gamma_u, \gamma_v} \sum_{\gamma_\mu, \gamma_\nu} \sum_{\gamma_i} (\Gamma_\nu, \gamma_\nu; \Gamma_i, \gamma_i | \Gamma_v, \gamma_v, r_v) \\ &\times (\Gamma_\mu, \gamma_\mu; \Gamma_i, \gamma_i | \Gamma_u, \gamma_u, r_u)^* (\Gamma_a, \gamma_a; \Gamma_v, \gamma_v | \Gamma_u, \gamma_u, r_u) (\Gamma_a, \gamma_a; \Gamma_\nu, \gamma_\nu | \Gamma_\mu, \gamma_\mu, r_\mu)^*. \end{aligned} \quad (.8)$$

In order to compute the spectral function, we also need  $\langle m_{u'} || f_{m_\alpha}^\dagger || m_{v'} \rangle_{(N)}$ , where  $f_{m_\alpha}^\dagger$  creates an electron at the one-electron impurity state  $|\alpha\rangle$  and  $m_{u'}$

are  $m_{v'}$  are the multiplets obtained after the diagonalization in step  $n$ . The expression in this case is

$$\begin{aligned} \langle m_{u'} | |f_{m_\alpha}^\dagger | |m_{v'} \rangle_{(N)} = & (-1)^{N_\mu} \sum_{r_u, r_v} \left[ U_{r_u, r_{u'}}^{(N)}(\Gamma_u) \right]^* U_{r_v, r_{v'}}^{(N)}(\Gamma_v) \delta_{m_\mu, m_\nu} \\ & \times \langle m_i | |f_{m_\alpha}^\dagger | |m_j \rangle_{(N)} F(\Gamma_u, \Gamma_v, \Gamma_i, \Gamma_j, \Gamma_\mu, \Gamma_\alpha), \end{aligned} \quad (.9)$$

where the block matrix element is obtained in the previous step,  $\langle m_i | |f_{m_\alpha}^\dagger | |m_j \rangle_{(N)} = \langle m_{u'} | |f_{m_\alpha}^\dagger | |m_{v'} \rangle_{(N-1)}$ , and the coefficient  $F$  is a sum over Clebsch-Gordan coefficients,

$$\begin{aligned} F(\Gamma_u, \Gamma_v, \Gamma_i, \Gamma_j, \Gamma_\mu, \Gamma_\alpha) = & \frac{1}{\dim(\Gamma_u)} \sum_{\gamma_u, \gamma_v} \sum_{\gamma_i, \gamma_j} \sum_{\gamma_\mu} \sum_{\gamma_\alpha} (\Gamma_\mu, \gamma_\mu; \Gamma_j, \gamma_j | \Gamma_v, \gamma_v, r_v) \\ & \times (\Gamma_\mu, \gamma_\mu; \Gamma_i, \gamma_i | \Gamma_u, \gamma_u, r_u)^* (\Gamma_\alpha, \gamma_\alpha; \Gamma_v, \gamma_v | \Gamma_u, \gamma_u, r_u) (\Gamma_\alpha, \gamma_\alpha; \Gamma_j, \gamma_j | \Gamma_i, \gamma_i, r_i)^*. \end{aligned} \quad (.10)$$

Our code precomputes the the coefficients  $D$ ,  $K$  and  $F$  for a set of irrep combinations chosen so that they cover all the possible inputs of a given NRG run. In this way, all the information about the structure of each irrep can be accessed at every step with very little computational cost.

## References

- [1] K. G. Wilson, The renormalization group: Critical phenomena and the kondo problem, *Rev. Mod. Phys.* 47 (1975) 773–840.
- [2] A. C. Hewson, *The Kondo problem to heavy fermions*, Cambridge University Press, 1993.
- [3] V. L. Campo, L. N. Oliveira, Alternative discretization in the numerical renormalization-group method, *Phys. Rev. B* 72 (2005) 104432.
- [4] R. Žitko, Adaptive logarithmic discretization for numerical renormalization group methods, *Computer Physics Communications* 180 (2009) 1271–1276.
- [5] M. Yoshida, M. A. Whitaker, L. N. Oliveira, Renormalization-group calculation of excitation properties for impurity models, *Phys. Rev. B* 41 (1990) 9403–9414.

- [6] W. C. Oliveira, L. N. Oliveira, Generalized numerical renormalization-group method to calculate the thermodynamical properties of impurities in metals, *Phys. Rev. B* 49 (1994) 11986–11994.
- [7] H. R. Krishna-Murthy, J. W. Wilkins, K. G. Wilson, Renormalization-group approach to the Anderson model of dilute magnetic alloys. I. Static properties for the symmetric case, *Physical Review B* 21 (1980) 1003–1043.
- [8] C. P. Moca, A. Alex, J. von Delft, G. Zaránd, SU(3) Anderson impurity model: A numerical renormalization group approach exploiting non-Abelian symmetries, *Physical Review B* 86 (2012) 195128.
- [9] M. Filippone, C. P. Moca, G. Zaránd, C. Mora, Kondo temperature of SU(4) symmetric quantum dots, *Physical Review B* 90 (2014) 121406.
- [10] D. Mantelli, C. Pacscu Moca, G. Zaránd, M. Grifoni, Kondo effect in a carbon nanotube with spin–orbit interaction and valley mixing: A DM-NRG study, *Physica E: Low-dimensional Systems and Nanostructures* 77 (2016) 180–190.
- [11] A. Weichselbaum, Non-abelian symmetries in tensor networks: A quantum symmetry space approach, *Annals of Physics* 327 (2012) 2972–3047.
- [12] O. Sakai, Y. Shimizu, T. Kasuya, Single-particle and magnetic excitation spectra of degenerate anderson model with finite f–f coulomb interaction, *Journal of the Physical Society of Japan* 58 (1989) 3666–3678.
- [13] R. Žitko, T. Pruschke, Energy resolution and discretization artifacts in the numerical renormalization group, *Phys. Rev. B* 79 (2009) 085106.
- [14] PointGroupNRG, <https://github.com/aitorcf/PointGroupNRG>, 2023.
- [15] The Julia Programming Language, <https://julialang.org/>, 2023.
- [16] M. Hamermesh, *Group theory and its application to physical problems*, Dover Publications, 1989.
- [17] W. K. Tung, *Group theory in physics*, World Scientific, 1985.

- [18] M. S. Dresselhaus, G. Dresselhaus, A. Jorio, *Group Theory: Application to the Physics of Condensed Matter*, Springer Berlin, Heidelberg, 2008.
- [19] J. Bünemann, F. Gebhard, Coulomb matrix elements in multi-orbital Hubbard models, *Journal of Physics: Condensed Matter* 29 (2017) 165601.
- [20] K. Chen, C. Jayaprakash, X-ray-edge singularities with nonconstant density of states: A renormalization-group approach, *Phys. Rev. B* 52 (1995) 14436–14440.
- [21] M. A. Ruderman, C. Kittel, Indirect Exchange Coupling of Nuclear Magnetic Moments by Conduction Electrons, *Phys. Rev.* 96 (1954) 99–102.
- [22] T. Kasuya, A Theory of Metallic Ferro- and Antiferromagnetism on Zener’s Model, *Progress of Theoretical Physics* 16 (1956) 45–57.
- [23] K. Yosida, Magnetic Properties of Cu-Mn Alloys, *Phys. Rev.* 106 (1957) 893–898.
- [24] O. Sakai, Y. Shimizu, T. Kasuya, Excitation spectra of two impurity anderson model, *Solid State Communications* 75 (1990) 81–87.
- [25] C. Jayaprakash, H. R. Krishna-murthy, J. W. Wilkins, Two-impurity kondo problem, *Phys. Rev. Lett.* 47 (1981) 737–740.
- [26] J. B. Silva, W. L. C. Lima, W. C. Oliveira, J. L. N. Mello, L. N. Oliveira, J. W. Wilkins, Particle-hole asymmetry in the two-impurity kondo model, *Phys. Rev. Lett.* 76 (1996) 275–278.
- [27] S. L. Altmann, P. Herzig, *Point-Group Theory Tables*, 2011.
- [28] C. Castellani, C. R. Natoli, J. Ranninger, Magnetic structure of  $v_2O_3$  in the insulating phase, *Phys. Rev. B* 18 (1978) 4945–4966.
- [29] L. Dworin, A. Narath, Orbital Paramagnetism of Localized Nonmagnetic Impurities in Metals, *Phys. Rev. Lett.* 25 (1970) 1287–1291.
- [30] A. Georges, L. d. Medici, J. Mravlje, Strong correlations from hund’s coupling, *Annual Review of Condensed Matter Physics* 4 (2013) 137–178.



- [31] M. A. Barral, S. Di Napoli, G. Blesio, P. Roura-Bas, A. Camjayi, L. O. Manuel, A. A. Aligia, Kondo behavior and conductance through 3d impurities in gold chains doped with oxygen, *The Journal of Chemical Physics* 146 (2017).
- [32] J. R. Schrieffer, P. A. Wolff, Relation between the Anderson and Kondo Hamiltonians, *Phys. Rev.* 149 (1966) 491–492.
- [33] R. Zitko, NRG Ljubljana (8f90ac4), Zenodo (2001). doi:<https://doi.org/10.5281/zenodo.4841076>.
- [34] J. Skolimowski, D. Vollhardt, K. Byczuk, Multitude of phases in correlated lattice fermion systems with spin-dependent disorder, *Journal of Physics Communications* 2 (2018) 025031.
- [35] H. Huang, S. Karan, B. Padurariu, Ciprian Kubala, J. C. Cuevas, J. Ankerhold, K. Kern, C. R. Ast, Universal scaling of tunable Yu-Shiba-Rusinov states across the quantum phase transition, *Communications Physics* 6 (2023).
- [36] M. Zonda, V. Pokorný, V. Janiš, T. Novotný, Perturbation theory of a superconducting  $0 - \pi$  impurity quantum phase transition, *Scientific Reports* 5 (2015).
- [37] R. Requist, S. Modesti, P. P. Baruselli, A. Smogunov, Kondo conductance across the smallest spin 1/2 radical molecule, *Proceedings of the National Academy of Sciences* 111 (2014) 69–74.
- [38] Packagecompiler.jl, <https://julialang.github.io/PackageCompiler.jl/stable/>, 2023.
- [39] Garbage collection in julia, <https://docs.julialang.org/en/v1/devdocs/gc/>, 2023.
- [40] P. P. Baruselli, R. Requist, A. Smogunov, M. Fabrizio, E. Tosatti, Co adatoms on Cu surfaces: Ballistic conductance and Kondo temperature, *Phys. Rev. B* 92 (2015) 045119.
- [41] P. P. Baruselli, M. Fabrizio, A. Smogunov, R. Requist, E. Tosatti, Magnetic impurities in nanotubes: From density functional theory to Kondo many-body effects, *Phys. Rev. B* 88 (2013) 245426.

- [42] S. Di Napoli, M. A. Barral, P. Roura-Bas, L. O. Manuel, A. M. Llois, A. A. Aligia, Kondo physics in a Ni impurity embedded in O-doped Au chains, *Phys. Rev. B* 92 (2015) 085120.
- [43] G. G. Blesio, L. O. Manuel, A. A. Aligia, P. Roura-Bas, Fully compensated Kondo effect for a two-channel spin  $S = 1$  impurity, *Phys. Rev. B* 100 (2019) 075434.
- [44] Y. Tanaka, N. Kawakami, A. Oguri, Crossover between two different Kondo couplings in side-coupled double quantum dots, *Phys. Rev. B* 85 (2012) 155314.
- [45] D. B. Karki, C. Mora, J. von Delft, M. N. Kiselev, Two-color Fermi-liquid theory for transport through a multilevel Kondo impurity, *Phys. Rev. B* 97 (2018) 195403.
- [46] X.-W. Chen, G.-Y. Yi, L.-L. Zhang, W.-B. Cui, W.-J. Gong, Kondo physics in the t-shaped structure with two detuned quantum dots, *Physica E: Low-dimensional Systems and Nanostructures* 134 (2021) 114928.